Directional outlyingness for multivariate functional data

Wenlin Dai *, Marc G. Genton

Statistics Program, King Abdullah University of Science and Technology, Thuwal 23955-6900, Saudi Arabia

ABSTRACT

The direction of outlyingness is crucial to describing the centrality of multivariate functional data. Motivated by this idea, classical depth is generalized to directional outlyingness for functional data. Theoretical properties of functional directional outlyingness are investigated and the total outlyingness can be naturally decomposed into two parts: magnitude outlyingness and shape outlyingness which represent the centrality of a curve for magnitude and shape, respectively. This decomposition serves as a visualization tool for the centrality of curves. Furthermore, an outlier detection procedure is proposed based on functional directional outlyingness. This criterion applies to both univariate and multivariate curves and simulation studies show that it outperforms competing methods. Weather and electrocardiogram data demonstrate the practical application of our proposed framework.

© 2018 Elsevier B.V. All rights reserved.

1. Introduction

Functional data are frequently observed in various fields of science, including but not limited to meteorology, biology, medicine, and engineering. Examples of functional data are temperature records from weather stations, curves capturing infant growth, expression levels of genes recorded over time, and hand-writing data, to name but a few. Over the past two decades, much work has been done that analyzes functional data, among which Ramsay and Silverman (2005) provided various parametric methods, Ferraty and Vieu (2006) developed detailed nonparametric techniques, and Horváth and Kokoszka (2012) focused on related inferential methods for functional data. Typically, each observation is a real function, either univariate or multivariate, defined on an interval, $\mathcal{I}$, in $\mathbb{R}$.

Statistical depth is widely utilized in nonparametric inference for functional data, for instance, to estimate the trimmed mean (Fraiman and Muniz, 2001), to classify functional data (López-Pintado and Romo, 2006), to construct the functional boxplots (Sun and Genton, 2011), and to detect outlying curves (Arribas-Gil and Romo, 2014; Hubert et al., 2015). It provides adequate tools for exploratory analysis of functional data in different scientific areas such as human health (McKeague et al., 2011), medical science (Hong et al., 2014), and neural science (Ngo et al., 2015).

The concept of statistical depth was initially proposed to rank multivariate data. Afterwards, it was generalized to provide an ordering from the center outwards of functional data. Existing depth functions for functional data include integrated depth (ID; Fraiman and Muniz, 2001), h-mode and random projection depth (Cuevas et al., 2006), random Tukey depth and integrated dual depth (Cuevas and Fraiman, 2009), band depth and modified band depth (BD and MBD; López-Pintado and Romo, 2009), half-region depth and modified half-region depth (HD and MHD; López-Pintado and Romo, 2011), spatial depth (Chakraborty and Chaudhuri, 2014b; Serfling and Wijesuriya, 2017), L^∞ depth (Long and Huang, 2015), extremal depth (Narisetty and Nair, 2016; Myllymäki et al., 2017), and total variation depth (Huang and Sun, 2016) for univariate functional

---

* Corresponding author.
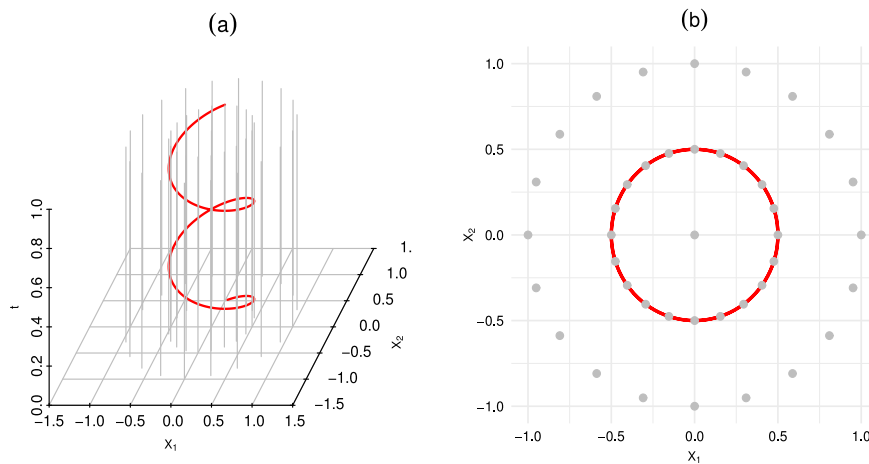 *E-mail address:* wenlin.dai@kaust.edu.sa (W. Dai).

(a) (b)

Fig. 1. (a) Forty-one normal curves (gray) and one outlier (red); (b) Projection of curves along the direction of the t-axis. Classical integrated functional depth cannot distinguish between the red and gray curves.

data; weighted modified band depth (WMBD; Ieva and Paganoni, 2013), simplicial band depth and modified simplicial band depth (SBD and MSBD; López-Pintado et al., 2014), multivariate functional halfspace depth (MFHD; Claeskens et al., 2014), and multivariate functional skew-adjusted projection depth (MFSPD; Hubert et al., 2015) for multivariate functional data. Chakraborty and Chaudhuri (2014a) investigated the "degeneracy" problem and proved that all curves may have zero depth with probability one in infinite-dimensional function spaces for some existing functional depths (like BD and HD). Nieto-Reyes and Battey (2016) proposed a formal definition of statistical depth for functional data from a topological point of view. Gijbels and Nagy (2015) and Nagy et al. (2016a, b) investigated the consistency of non-integrated and integrated depths for functional data, respectively.

Outlier detection is often a necessary step in preliminary analysis of functional data. Handling a variety of functional outliers including persistent outliers that are outlying on a large part of the domain, isolated outliers that are outlying for a very short time interval, magnitude outliers and shape outliers, can be challenging; see Hubert et al. (2015). Many outlier detection methods for functional data have been developed based on functional depth. Febrero et al. (2008) defined outliers as those curves with depths smaller than a threshold generated through a bootstrap procedure. Hyndman and Shang (2010) proposed several visualization tools and made a comparison of some outlier detection methods for functional data. Sun and Genton (2011) proposed a now-popular visualization and outlier detection tool named *functional boxplot*; this tool is based on MBD but the band depth can be replaced by other functional depths. Gervini (2012) detected outliers using boxplots or histograms of a measure of outlyingness. Arribas-Gil and Romo (2014) proposed an *outliergram* that detects shape outliers by connecting two functional depths. Hubert et al. (2015) presented a taxonomy of functional outliers and proposed two visualization methods for outlier detection. Apart from these depth-based methods, other criteria have also been proposed for detecting outliers in functional data (Gervini, 2009; Hyndman and Shang, 2010; Yu et al., 2012).

Most existing functional depths, for instance, ID, MBD, MHD, MSBD, MFHD, and MFSPD, fall into the category of integrated functional depth: weighted average of point-wise depth. These point-wise depths are always non-negative scalars in the interval [0, 1], with large depths assigned to central points and small depths assigned to outward ones. However, we have found that this type of depths cannot efficiently describe the centrality of functions. The following example illustrates this deficiency: 42 bivariate curves are defined on $t \in [0, 1]$. Among these curves, 41 gray lines take fixed values across [0, 1]: (0, 0), $\{0.5 \sin(i\pi/10), 0.5 \cos(i\pi/10)\}$, and $\{\sin(i\pi/10), \cos(i\pi/10)\}$, $i = 1, \ldots, 20$, respectively, and a red curve is $\{0.5 \sin(t\pi/10), 0.5 \cos(t\pi/10)\}$; see Fig. 1(a). When we project these curves along the t direction, we get Fig. 1(b). Clearly, the red curve is very different from the other curves. It should thus have a smaller depth and be recognized as an outlier. However, the red curve and the 20 straight lines on the smaller circle actually share the same depth value for some existing functional depths, such as MSBD and MFHD, because they always get the same point-wise depth at each time point t. What makes the red curve an outlier is the change of the direction of outlyingness, which unfortunately has never been considered in existing definitions of functional depths from the literature.

To effectively distinguish the red curve from the gray curves, a natural idea is to consider the direction of outlyingness in addition to the point-wise scalar depth. Bearing this purpose in mind, we propose the framework of directional outlyingness for multivariate functional data, and demonstrate that the new framework enjoys the following three advantages:

1. Functional directional outlyingness is applicable to both univariate and multivariate functional data with one- or multi-dimensional design domains;
2. Functional directional outlyingness decomposes functional outlyingness into two natural parts: *magnitude outlyingness* and *shape outlyingness*; it provides a much better description of the centrality of curves and the variability among them;

3. An outlier detection criterion is constructed based on functional directional outlyingness; this criterion outperforms existing methods for effectively detecting various types of outliers.

The remainder of this paper is organized as follows. In Section 2, we propose the framework of directional outlyingness for multivariate functional data. In Section 3, we derive an outlyingness decomposition from functional directional outlyingness and visually compare it with classical functional depths. Also, we study important properties and consistency of functional directional outlyingness. In Section 4, we construct an outlier detection procedure for functional data based on functional directional outlyingness. In Section 5, we evaluate the proposed outlier detection procedure with Monte Carlo simulation studies for both univariate and multivariate functional data. We analyze two data examples using our proposed framework in Section 6. We end the paper with a discussion in Section 7. Proofs of the theoretical results are provided in Appendix A.

2. Functional directional outlyingness

Consider a stochastic process, $\mathbf{X} : \mathcal{I} \longrightarrow \mathbb{R}^p$, that takes values in the space $\mathcal{C}(\mathcal{I}, \mathbb{R}^p)$ of real continuous functions defined from a compact interval, $\mathcal{I}$, to $\mathbb{R}^p$ with probability distribution $F_{\mathbf{X}}$. At each fixed time point, $t \in \mathcal{I}$, $\mathbf{X}(t)$ is a p-variate random variable with probability distribution $F_{\mathbf{X}(t)}$. Here, p is a finite positive integer that indicates the dimension of the functional data: we get univariate functional data when $p = 1$ and multivariate functional data when $p \geq 2$.

Unlike most existing functional depths utilizing statistical depth, our measure of centrality for functional data is built on the concept of *outlyingness*. For multivariate data, outlyingness functions are equivalent to statistical depths in an inverse sense (Serfling, 2006). For functional data, outlyingness turns out to be a better choice, as we demonstrate in the next section. Let $d(\mathbf{X}(t), F_{\mathbf{X}(t)}): \mathbb{R}^p \longrightarrow [0, 1]$ be a statistical depth function for $\mathbf{X}(t)$ with respect to $F_{\mathbf{X}(t)}$. Denote the outlyingness of $\mathbf{X}(t)$ with respect to $F_{\mathbf{X}(t)}$ with $o(\mathbf{X}(t), F_{\mathbf{X}(t)})$. The connections among depth, outlyingness, quantile, and rank functions for multivariate data have been comprehensively studied by Zuo and Serfling (2000) and Serfling (2006, 2010). Generally, these two quantities can be connected via

$$d(\mathbf{X}(t), F_{\mathbf{X}(t)}) = \{1 + o(\mathbf{X}(t), F_{\mathbf{X}(t)})\}^{-1}, \tag{1}$$

when $o(\mathbf{X}(t), F_{\mathbf{X}(t)})$ has a range $[0, \infty)$, or alternatively via

$$d(\mathbf{X}(t), F_{\mathbf{X}(t)}) = 1 - o(\mathbf{X}(t), F_{\mathbf{X}(t)})/\{\sup o(\cdot, F_{\mathbf{X}(t)})\} \tag{2}$$

when $o(\mathbf{X}(t), F_{\mathbf{X}(t)})$ is bounded. Serfling (2006) introduced three ways to constructing outlyingness for point-type data: projection pursuit approach, distance approach, and quantile function approach. Most existing depths can be derived from their corresponding outlyingness; see Zuo and Serfling (2000) and Serfling (2006) for discussions.

To capture the magnitude as well as the direction of outlyingness, we introduce directional outlyingness for multivariate data as follows:

$$\mathbf{O}(\mathbf{X}(t), F_{\mathbf{X}(t)}) = o(\mathbf{X}(t), F_{\mathbf{X}(t)}) \cdot \mathbf{v}(t) = \left\{ 1/d(\mathbf{X}(t), F_{\mathbf{X}(t)}) - 1 \right\} \cdot \mathbf{v}(t), \tag{3}$$

where $d(\mathbf{X}(t), F_{\mathbf{X}(t)}) > 0$, $\mathbf{v}(t) = \{\mathbf{X}(t) - \mathbf{Z}(t)\} / \|\mathbf{X}(t) - \mathbf{Z}(t)\|$ is the spatial sign (Möttönen and Oja, 1995) of $\{\mathbf{X}(t) - \mathbf{Z}(t)\}$, $\mathbf{Z}(t)$ denotes the unique median of the distribution $F_{\mathbf{X}(t)}$ with respect to $d(\mathbf{X}(t), F_{\mathbf{X}(t)})$, and $\| \cdot \|$ denotes the L_2 norm. Here, the magnitude of directional outlyingness is defined based on statistical depth via the connection (1). A similar concept in the literature is the centered rank function, $\mathbf{R}(\mathbf{X}(t), F_{\mathbf{X}(t)})$, proposed by Serfling (2010), which is the inverse of a multivariate quantile function $\mathbf{Q}(\mathbf{X}(t), F_{\mathbf{X}(t)})$. Obviously, the directional outlyingness is different from the centered rank function: $\mathbf{O}(\mathbf{X}(t), F_{\mathbf{X}(t)})$ takes values in $\mathbb{R}^p$ whereas $\mathbf{R}(\mathbf{X}(t), F_{\mathbf{X}(t)})$ takes values in the unit ball $\mathbb{B}^{p-1}(\mathbf{0}) \in \mathbb{R}^p$ (Serfling, 2010). For ranking multivariate data, the two quantities are equivalent; however, directional outlyingness is more flexible for ranking functional data. Accordingly, the empirical directional outlyingness is defined as $\mathbf{O}_n(\mathbf{X}(t), F_{\mathbf{X}(t),n}) = \{1/d_n(\mathbf{X}(t), F_{\mathbf{X}(t),n}) - 1\} \cdot \mathbf{v}_n(t)$, where $\mathbf{v}_n(t)$ is the unit vector pointing from $\mathbf{Z}_n(t)$ to $\mathbf{X}(t)$ and $\mathbf{Z}_n(t)$ stands for the median of $\{\mathbf{X}_1(t), \ldots, \mathbf{X}_n(t)\}$ with respect to the empirical depth $d_n(\mathbf{X}(t), F_{\mathbf{X}(t),n})$. For the case that $\mathbf{Z}_n(t)$ is not unique, we average all the medians as the unique median for defining $\mathbf{v}_n(t)$.

Classical depth projects $\mathbf{X}(t)$ onto $[0, 1] \subset \mathbb{R}$, whereas directional outlyingness projects $\mathbf{X}(t)$ onto $\mathbb{R}^p$. We provide an example for the case $p = 2$ and calculate the simplicial depth (SD; Liu, 1990) and the directional Stahel–Donoho outlyingness (SDO; Stahel, 1981; Donoho, 1982) for each point to illustrate their difference (Fig. 2, left column). In comparing classical depth and directional outlyingness, we observe that directional outlyingness retains data positions relative to the median, clearly separating the outliers, whereas simplicial depth projects all the outliers onto the left boundary of the plot and consequently mixes them up. We derive properties of directional outlyingness and present them in the following theorems.

Theorem 1. *For a fixed time point $t_0 \in \mathcal{I}$, assume that $d\left(\mathbf{X}(t_0), F_{\mathbf{X}(t_0)}\right) > 0$ is a valid depth function with respect to Definition 2.1 in* Zuo and Serfling (2000)*, which means that it possesses four properties: affine invariance, maximality at the center, monotonicity relative to the deepest point and invisibility at infinity. Then, the associated directional outlyingness, $\mathbf{O}\left(\mathbf{X}(t_0), F_{\mathbf{X}(t_0)}\right)$, satisfies the following properties:*

(i) *Affine invariance:* $\mathbf{O}\left(\mathbf{A}\mathbf{X}(t_0) + \mathbf{b}, F_{\mathbf{A}\mathbf{X}(t_0)+\mathbf{b}}\right) = \mathbf{U} \cdot \mathbf{O}\left(\mathbf{X}(t_0), F_{\mathbf{X}(t_0)}\right)$ *holds for any* $p \times p$ *nonsingular matrix,* $\mathbf{A}$, *and any p-vector,* $\mathbf{b}$, *where* $\mathbf{U} = \mathbf{A}\|\mathbf{X}(t_0) - \mathbf{Z}(t_0)\|/\|\mathbf{A}\{\mathbf{X}(t_0) - \mathbf{Z}(t_0)\}\|$. *For the norm, we have* $\|\mathbf{O}\left(\mathbf{A}\mathbf{X}(t_0) + \mathbf{b}, F_{\mathbf{A}\mathbf{X}(t_0)+\mathbf{b}}\right)\| = \|\mathbf{O}\left(\mathbf{X}(t_0), F_{\mathbf{X}(t_0)}\right)\|$.

(ii) *Minimality at the center: For any* $F_{\mathbf{X}(t_0)}$ *with a unique median,* $\mathbf{Z}(t_0)$, $\|\mathbf{O}\left(\mathbf{Z}(t_0), F_{\mathbf{X}(t_0)}\right)\| = \inf_{\mathbf{X}(t_0)\in\mathbb{R}^p}\|\mathbf{O}\left(\mathbf{X}(t_0), F_{\mathbf{X}(t_0)}\right)\| = 0$.

(iii) *Monotonicity relative to the deepest point: For any* $F_{\mathbf{X}(t_0)}$ *with deepest point* $\mathbf{Z}(t_0)$, $\|\mathbf{O}\left(\mathbf{Z}(t_0), F_{\mathbf{X}(t_0)}\right)\| \leq \|\mathbf{O}\big(\mathbf{Z}(t_0) + \alpha\{\mathbf{X}(t_0) - \mathbf{Z}(t_0)\}, F_{\mathbf{X}(t_0)}\big)\|$ *holds for any* $\alpha \in [0, 1]$.

When $\mathbf{A}$ is an orthogonal matrix, $\|\mathbf{X}(t_0) - \mathbf{Z}(t_0)\| = \|\mathbf{A}\{\mathbf{X}(t_0) - \mathbf{Z}(t_0)\}\|$ and we can rewrite property (i) as $\mathbf{O}\left(\mathbf{A}\mathbf{X}(t_0) + \mathbf{b}, F_{\mathbf{A}\mathbf{X}(t_0)+\mathbf{b}}\right) = \mathbf{A} \cdot \mathbf{O}\left(\mathbf{X}(t_0), F_{\mathbf{X}(t_0)}\right)$.

Theorem 2. *For a fixed time point* $t_0 \in \mathcal{I}$, *assume that*

$$\sup_{\mathbf{X}(t_0)\in\mathbb{R}^p} |d_n\left(\mathbf{X}(t_0), F_{\mathbf{X}(t_0),n}\right) - d\left(\mathbf{X}(t_0), F_{\mathbf{X}(t_0)}\right)| \to 0 \ a.s.$$

and $\mathbf{Z}_n(t_0) \to \mathbf{Z}(t_0)$ *as* $n \to \infty$. *Then directional outlyingness is consistent:*

$$\sup_{\mathbf{X}(t_0)\in\mathbb{R}^p} \left\|\mathbf{O}_n\left(\mathbf{X}(t_0), F_{\mathbf{X}(t_0),n}\right) - \mathbf{O}\left(\mathbf{X}(t_0), F_{\mathbf{X}(t_0)}\right)\right\| \to 0 \quad a.s. \quad \text{as } n \to \infty.$$

With the above directional outlyingness for multivariate data, we propose descriptive statistics for functional data. We show that the direction of outlyingness significantly enhances the classical functional depth for illustrating the centrality of functional data.

Definition 1. Consider a stochastic process, $\mathbf{X} : \mathcal{I} \longrightarrow \mathbb{R}^p$, that takes values in the space $\mathcal{C}(\mathcal{I}, \mathbb{R}^p)$ of real continuous functions defined from a compact interval, $\mathcal{I}$, to $\mathbb{R}^p$ with probability distribution $F_{\mathbf{X}}$. Let $\mathbf{O}$ be the directional outlyingness defined as (3) and $w(t)$ a weight function on $\mathcal{I}$. Further assume that, for $t \in \mathcal{I}$, $\mathbf{O}(\mathbf{X}(t), F_{\mathbf{X}(t)})$ is square integrable. We have the following definitions: functional directional outlyingness (FO),

$$\text{FO}(\mathbf{X}, F_{\mathbf{X}}) = \int_{\mathcal{I}} \|\mathbf{O}(\mathbf{X}(t), F_{\mathbf{X}(t)})\|^2 w(t)\mathrm{d}t;$$

mean directional outlyingness (**MO**),

$$\mathbf{MO}(\mathbf{X}, F_{\mathbf{X}}) = \int_{\mathcal{I}} \mathbf{O}(\mathbf{X}(t), F_{\mathbf{X}(t)})w(t)\mathrm{d}t;$$

and variation of directional outlyingness (VO),

$$\text{VO}(\mathbf{X}, F_{\mathbf{X}}) = \int_{\mathcal{I}} \|\mathbf{O}(\mathbf{X}(t), F_{\mathbf{X}(t)}) - \mathbf{MO}(\mathbf{X}, F_{\mathbf{X}})\|^2 w(t)\mathrm{d}t.$$

Here FO represents the *total outlyingness* of $\mathbf{X}$, similar to the classical functional depth. Next, **MO** describes the relative position (including both distance and direction) of $\mathbf{X}$ on average to the center curve and $\|\mathbf{MO}\|$ can be regarded as the *magnitude outlyingness* of $\mathbf{X}$. Finally, VO measures the change of $\mathbf{O}(\mathbf{X}(t), F_{\mathbf{X}(t)})$ in terms of both norm and direction across the whole design interval and can be regarded as the *shape outlyingness* of $\mathbf{X}$. Unlike classical functional depth, our functional directional outlyingness is no longer a single scalar. Classical functional depth (fd) is a mapping $\mathbf{X} \in \mathcal{C}(\mathcal{I}, \mathbb{R}^p) \longrightarrow \text{fd} \in [0, 1]$, whereas functional directional outlyingness is a mapping $\mathbf{X} \in \mathcal{C}(\mathcal{I}, \mathbb{R}^p) \longrightarrow (\mathbf{MO}^{\mathrm{T}}, VO)^{\mathrm{T}} \in \mathbb{R}^p \times \mathbb{R}^+$, which greatly enlarges our flexibility of analyzing curves. The weight function, $w(t)$, can be a constant function (Fraiman and Muniz, 2001; López-Pintado et al., 2014), or proportional to the amount of local variability in amplitude (Claeskens et al., 2014). Throughout this paper, we use a constant weight function, $w(t) = \{\lambda(\mathcal{I})\}^{-1}$, where $\lambda(\cdot)$ represents the Lebesgue measure. The finite sample versions of descriptive statistics in Definition 1 are defined by replacing $F_{\mathbf{X}(t)}$ and $F_{\mathbf{X}}$ with their empirical versions, $F_{\mathbf{X}(t),n}$ and $F_{\mathbf{X},n}$, respectively. For example,

$$\mathbf{MO}_n(\mathbf{X}, F_{\mathbf{X},n}) = \int_{\mathcal{I}} \mathbf{O}_n(\mathbf{X}(t), F_{\mathbf{X}(t),n}) \cdot w_n(t)\mathrm{d}t,$$

where $w_n(t)$ is the finite sample version of the chosen weight function and other quantities can be defined accordingly.

Different depth notions can be utilized to define functional directional outlyingness. We generally divide point-wise depths into two classes according to their dependence on either rank or distance information. The first class contains rank-based depths and includes half-region depth (Tukey, 1975) and simplicial depth (SD; Liu, 1990) among others; the second class contains distance-based depths and includes Mahalanobis depth (Mahalanobis, 1936), spatial depth (Vardi and Zhang, 2000) and projection depth (PD; Zuo, 2003) among others. Through our investigation, we find that a distance-based depth is more appropriate for constructing directional outlyingness because it involves more information than a rank-based depth. In this paper, we use the projection depth (Zuo, 2003) to generate numerical results. Specifically, the projection depth is defined as

$$\text{PD}(\mathbf{X}(t), F_{\mathbf{X}(t)}) = \{1 + \text{SDO}(\mathbf{X}(t), F_{\mathbf{X}(t)})\}^{-1},$$

where

$$\text{SDO}(\mathbf{X}(t), F_{\mathbf{X}(t)}) = \sup_{\|\mathbf{u}\|=1} \frac{\|\mathbf{u}^{\mathsf{T}}\mathbf{X}(t) - \text{median}(\mathbf{u}^{\mathsf{T}}\mathbf{X}(t))\|}{\text{MAD}(\mathbf{u}^{\mathsf{T}}\mathbf{X}(t))}$$

is the Stahel–Donoho outlyingness (Stahel, 1981; Donoho, 1982). Following (3), the directional SDO (**dSDO**) is expressed as:

$$\mathbf{dSDO}(\mathbf{X}(t), F_{\mathbf{X}(t)}) = \text{SDO}(\mathbf{X}(t), F_{\mathbf{X}(t)}) \cdot \mathbf{v}(t).$$

Substituting **dSDO** into Definition 1, we get a Stahel–Donoho type of functional directional outlyingness (**dFSDO**).

3. Properties of functional directional outlyingness

This section introduces two theorems on the properties of functional directional outlyingness. In particular, we show that the proposed functional directional outlyingness provides a natural decomposition of the functional outlyingness. It also shares some similar properties with classical functional depth.

3.1. Functional outlyingness decomposition

Theorem 3. *For the proposed statistics in Definition 1, we have the following relationship:*

$$\text{FO}(\mathbf{X}, F_{\mathbf{X}}) = \|\mathbf{MO}(\mathbf{X}, F_{\mathbf{X}})\|^2 + \text{VO}(\mathbf{X}, F_{\mathbf{X}}). \tag{4}$$

Eq. (4) provides a decomposition of FO: total functional directional outlyingness is separated into two parts, magnitude outlyingness and shape outlyingness. When a group of curves shares the same shape or, equivalently, they are parallel to each other, we may expect that VO is close to zero. In that case, a quadratic relationship appears between FO and $\|\mathbf{MO}\|$. In contrast, classical depth cannot be decomposed in this way because it does not contain the information of the direction. To illustrate this difference, we provide examples for both univariate and bivariate curves (Fig. 2, middle and right columns).

For the univariate case, we generate a sample of curves with different types of outliers and compare the MBD with the **dFSDO** of each curve (Fig. 2, middle column). Five outliers are presented in different colors, including two pure magnitude outliers (red and blue), two pure shape outliers (cyan and purple), and one outlier (green) that is outlying for both magnitude and shape. Two shifted outliers are all mapped to the left edge of the plot and are not easy to be distinguished from the normal curves on the boundary for MBD, whereas, they are well separated by their much larger MO from **dFSDO**. Also, the two shape outliers for MBD are extensively covered with normal curves, whereas they are clearly isolated from the normal curves by their larger VO from **dFSDO**. This again indicates that the shape outlyingness (VO) is actually an effective measure of the variation in the shape of a curve. Moreover, MBD only demonstrates the green curve's outlyingness for magnitude and cannot tell the difference between the green and red curves. In contrast, **dFSDO** comprehensively illustrates the green curve's outlyingness for magnitude and shape: a smaller MO stands for its downward shift and a larger VO stands for its different shape. We compare the MFHD and the **dFSDO** of the bivariate case (Fig. 2, right column) and observe similar improvements. Overall, with the functional directional outlyingness and the decomposition (4), we obtain a much better visualization of the curves with respect to the centrality.

3.2. Theoretical properties

Now assume that $\mathcal{I}$ is a compact interval, that the distribution $F_{\mathbf{X}}$ is absolutely continuous and that $F_{\mathbf{X}(t)}$ has a unique median, $\mathbf{Z}(t)$, for each $t \in \mathcal{I}$. We investigate the properties of functional directional outlyingness and present them in the following theorem.

Theorem 4. *Assume that $\mathbf{O}(\mathbf{X}(t), F_{\mathbf{X}(t)})$ is a directional outlyingness from Theorem 1. Then, **MO**, VO and FO in Definition 1 possess the following properties:*

1. *Transformation invariance:*

   (a) *Let $\mathbf{T}(\mathbf{X})$ be a functional, $\mathcal{C}(\mathcal{I}, \mathbb{R}^p) \longrightarrow \mathcal{C}(\mathcal{I}, \mathbb{R}^p)$, with the form $\mathbf{T}(\mathbf{X}(t)) = \mathbf{A}(t)\mathbf{X}(t) + \mathbf{b}(t)$, where $\mathbf{A}(t)$ is a nonsingular matrix and $\mathbf{b}(t)$ is a p-vector for each $t \in \mathcal{I}$. In addition, let g be a bijection on the interval, $\mathcal{I}$, and let the weight function, $w(t)$, be a constant function. Then,*

   $$\text{FO}\left(\mathbf{T}(\mathbf{X}_g), F_{\mathbf{T}(\mathbf{X}_g)}\right) = \text{FO}\left(\mathbf{X}, F_{\mathbf{X}}\right),$$

   where $\mathbf{X}_g(t) = \mathbf{X}(g(t))$ for each $t \in \mathcal{I}$.

   (b) *Moreover, if we further assume that $\mathbf{A}(t) = f(t)\mathbf{A}_0$, where $f(t) > 0$ for $t \in \mathcal{I}$ and $\mathbf{A}_0$ is an orthogonal matrix, then we have*

   $$\mathbf{MO}\left(\mathbf{T}(\mathbf{X}_g), F_{\mathbf{T}(\mathbf{X}_g)}\right) = \mathbf{A}_0 \cdot \mathbf{MO}\left(\mathbf{X}, F_{\mathbf{X}}\right),$$
   $$\text{VO}\left(\mathbf{T}(\mathbf{X}_g), F_{\mathbf{T}(\mathbf{X}_g)}\right) = \text{VO}\left(\mathbf{X}, F_{\mathbf{X}}\right).$$
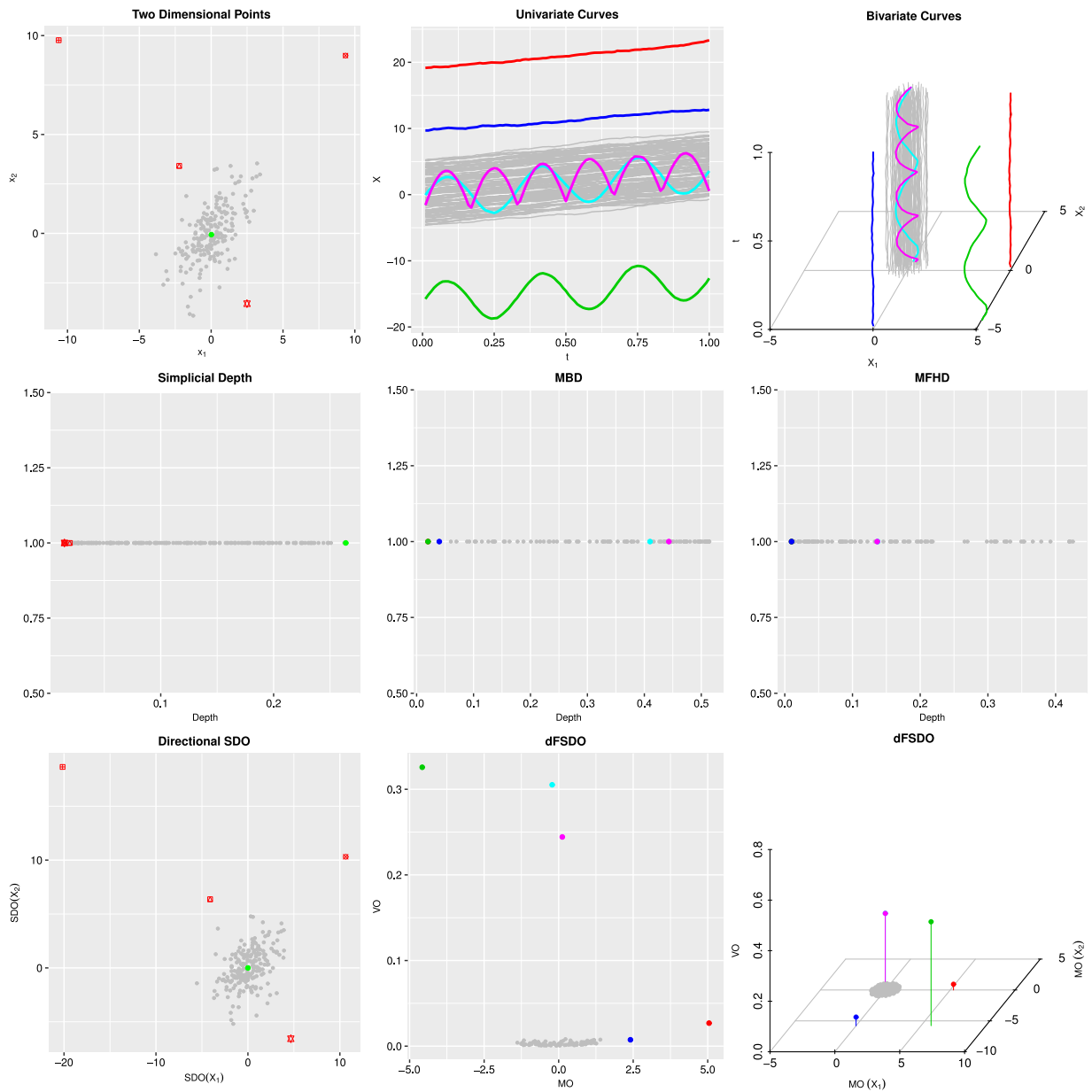
Fig. 2. Left column: scatter plot of 204 points generated from a normal distribution. The four red points are outliers and the green point is the median with respect to simplicial depth (top), simplicial depth (middle) and directional SDO (bottom). Middle column: 100 univariate curves (gray) with 5 outlying curves (various colors), MBD (middle) and directional functional SDO (**dFSDO**, bottom). Right column: 100 bivariate curves (gray) with 5 outlying curves (various colors), MFHD (middle) and **dFSDO** (bottom). (For interpretation of the references to color in this figure legend, the reader is referred to the web version of this article.)

2. *Minimality at the center:*

$$\mathrm{FO}\,(\mathbf{Z}, F_{\mathbf{X}}) = \inf_{\mathbf{X} \in \mathcal{C}(\mathcal{I}, \mathbb{R}^p)} \mathrm{FO}\,(\mathbf{X}, F_{\mathbf{X}})\,,$$

for any distribution, $F_{\mathbf{X}}$, with a unique center function of symmetry $\mathbf{Z}$.

3. *Monotonicity with respect to the deepest point:* Assume that $\mathbf{Z}$ exists for $F_{\mathbf{X}}$ such that $\mathbf{Z}(t)$ is the deepest point at every $t \in \mathcal{I}$. Then, for any $\alpha \in [0, 1]$, we have that

$$\mathrm{FO}\,(\mathbf{X}, F_{\mathbf{X}}) \geq \mathrm{FO}\,(\mathbf{X} + \alpha(\mathbf{Z} - \mathbf{X}), F_{\mathbf{X}})\,.$$

If we use an affine invariant weight function proportional to the local variability, we need to further assume that $\det\{\mathbf{A}(t)\}$ is a constant for each $t \in \mathcal{I}$ to guarantee the affine invariance of FO. This result is more general than Theorem 1 in Claeskens et al. (2014), which applies an identical transformation to $\mathbf{X}(t)$ at each time point.

In practice, we get observations only at a finite set of time points, say $T_k = \{t_1, t_2, \ldots, t_k\}$ in $\mathcal{I}$, for a finite sample of curves. Under this setting, we can also define some descriptive statistics as in Definition 1. For example, we may define

$$\mathbf{MO}_{T_k}(\mathbf{X}, F_\mathbf{X}) = \frac{1}{k} \sum_{i=1}^k \mathbf{O}\left(\mathbf{X}(t_i), F_{\mathbf{X}(t_i)}\right) w(t_i),$$

$$\mathbf{MO}_{T_k,n}\left(\mathbf{X}, F_{\mathbf{X},n}\right) = \frac{1}{k} \sum_{i=1}^k \mathbf{O}_n\left(\mathbf{X}(t_i), F_{\mathbf{X}(t_i),n}\right) w_n(t_i).$$

Finite dimensional versions can be defined similarly for the other four statistics.

Theorem 5. *For the finite-dimensional setting above, assume that the convergence of $\mathbf{O}_n$ holds as stated in Theorem 2 and that $w_n(t)$ converges almost surely to $w(t)$ as $n \to \infty$ for each $t \in T_k$. Then, we get the convergence of $\mathbf{MO}_{T_k,n}$ as*

$$\sup_{\mathbf{X} \in (\mathbb{R}^p)^k} \|\mathbf{MO}_{T_k,n}\left(\mathbf{X}, F_{\mathbf{X},n}\right) - \mathbf{MO}_{T_k}\left(\mathbf{X}, F_\mathbf{X}\right)\| \to 0 \quad a.s. \quad \text{as } n \to \infty.$$

When $k = k(n) \to \infty$, one can follow the proof of Theorem 3 in Claeskens et al. (2014) to obtain the consistency of $\mathbf{MO}_{T_k,n}\left(\mathbf{X}, F_{\mathbf{X},n}\right) \to \mathbf{MO}\left(\mathbf{X}, F_\mathbf{X}\right)$.

4. Functional outlier detection

Apart from better visualizing the centrality of curves, we can also design an outlier detection procedure with functional directional outlyingness. In the literature, a depth-based outlier detection procedure relies on either a cutoff of functional depth distribution chosen by bootstrap (Febrero et al., 2008) or an envelop constructed by central curves (Hyndman and Shang, 2010; Sun and Genton, 2011). In the current paper, we design our outlier detection method using $\mathbf{MO}_{T_k,n}$ and $\mathrm{VO}_{T_k,n}$ jointly.

Through our numerical studies, we found that the distribution of $\mathbf{Y}_{k,n} = (\mathbf{MO}_{T_k,n}^\mathrm{T}, \mathrm{VO}_{T_k,n})^\mathrm{T}$ can be well approximated with a $(p+1)$-dimensional normal distribution when $\mathbf{X}$ is generated from a p-dimensional stationary Gaussian process. As an example, we generated 500 curves at k equidistant points on $[0, 1]$ from the random process (denoted as Model 0): $X(t) = 4t + \epsilon(t)$, where $\epsilon(t)$ is a Gaussian process with zero mean and covariance function $r(s, t) = \exp\{-1000|t - s|\}$. We calculated $\mathbf{MO}_{T_k,n}$ and $\mathrm{VO}_{T_k,n}$ with different numbers of design points, $k = 1000$ and 10000. Then we computed the normal Q–Q plot trajectory of each quantity. We repeated this procedure 100 times and plot these trajectories under two settings; see Fig. 3. As shown, the two quantities are well approximated by the normal distribution under both settings.

Such an approximation allows us to use the results from Hardin and Rocke (2005) to detect potential outliers from $\mathbf{Y}_{k,n}$. In particular, we calculate the robust Mahalanobis distance of $\mathbf{Y}_{k,n}$ with Rousseeuw (1985)'s minimum covariance determinant estimators for shape and location of the data. Finally, we employ the approximation proposed by Hardin and Rocke (2005) for the distribution of these distances and determine the cutoff based on such an approximation. It turns out that this procedure is quite effective in the simulation studies. Specifically, the outlier detection is conducted by the following three steps:

1. Calculate the robust Mahalanobis distance based on a sample of size $h \le n$,

$$\mathrm{RMD}^2(\mathbf{Y}_{k,n}, \bar{\mathbf{Y}}_{k,n,J}^*) = (\mathbf{Y}_{k,n} - \bar{\mathbf{Y}}_{k,n,J}^*)^\mathrm{T} \mathbf{S}_{k,n,J}^{* -1}(\mathbf{Y}_{k,n} - \bar{\mathbf{Y}}_{k,n,J}^*),$$

   where J denotes the group of h points that minimizes the determinant of the corresponding covariance matrix, $\bar{\mathbf{Y}}_{k,n,J}^* = h^{-1} \sum_{i \in J} \mathbf{Y}_{k,n,i}$ and $\mathbf{S}_{k,n,J}^* = h^{-1} \sum_{i \in J} (\mathbf{Y}_{k,n,i} - \bar{\mathbf{Y}}_{k,n,J}^*)(\mathbf{Y}_{k,n,i} - \bar{\mathbf{Y}}_{k,n,J}^*)^\mathrm{T}$. The sub-sample of size h controls the robustness of the method. For a p-dimensional distribution, the maximum finite sample breakdown point is $[(n - p + 1)/2]/n$, where $[a]$ denotes the integer part of $a \in \mathbb{R}$.

2. According to the results in Hardin and Rocke (2005), approximate the tail of this distance distribution as follows:

$$\frac{c(m-p)}{m(p+1)} \mathrm{RMD}^2(\mathbf{Y}_{k,n}, \bar{\mathbf{Y}}_{k,n,J}^*) \sim F_{p+1,m-p},$$

   where c and m are parameters determining the degrees of freedom of the F-distribution and the scaling factor, respectively. They are calculated by a simulation program provided by Hardin and Rocke (2005). Then, we choose a cutoff value, C, as the α quantile of $F_{p+1,m-p}$. We set $\alpha = 0.993$, which is used in the classical boxplot for detecting outliers under a normal distribution.

3. Flag a curve as an outlier when its distance satisfies

$$\frac{c(m-p)}{m(p+1)} \mathrm{RMD}^2(\mathbf{Y}_{k,n}, \bar{\mathbf{Y}}_{k,n,J}^*) > C.$$

The RMD can also serve as a measure of centrality for the curves, based on which we can define the median and the central region of the curves, calculate the trimmed mean function, and generate the functional boxplot as well.
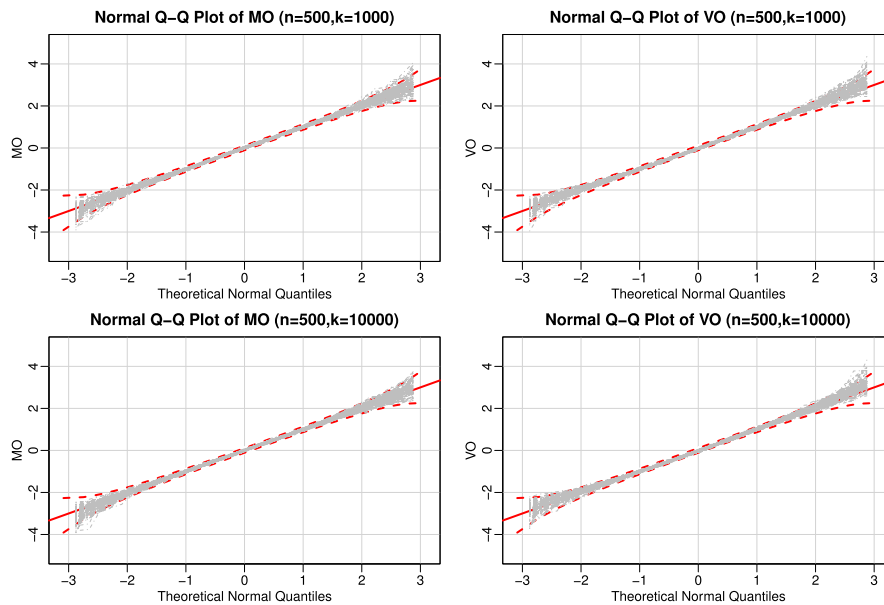
Fig. 3. 100 normal Q–Q plot trajectories (gray curves) of $\mathrm{MO}_{T_k,n}$ and $\mathrm{VO}_{T_k,n}$ under two settings of Model 0 are shown together with a 95% point-wise confidence envelop of the quantiles of the standard normal distribution. The red solid line: $y = x$. The two red dashed lines: upper and lower bounds of the confidence envelop. We have standardized the quantities and the theoretical quantiles are generated from the standard normal distribution. Top panel: $k = 1000$; bottom panel: $k = 10000$. Both $\mathrm{MO}_{T_k,n}$ and $\mathrm{VO}_{T_k,n}$ are well approximated by the normal distribution.

5. Monte Carlo simulation studies

We have demonstrated the superiority of directional outlyingness in describing and visualizing both point-wise and functional data. In this section, we conduct simulation studies to assess the performance of the proposed outlier detection procedure based on RMD, denoted as Dir.Out. Our simulation studies include both univariate and multivariate functional data. Throughout the simulations, we use a constant weight function for calculating **dFSDO**.

5.1. Univariate functional data

For univariate functional data, we compare Dir.Out with three existing methods:

1. Integrated squared error method (Int.Sqe; Hyndman and Ullah, 2007): the integrated squared error is calculated for each curve after extracting some fixed number of principal components. Outliers are defined as those observations with an integrated squared error greater than a threshold. We use *foutliers* in the R package *rainbow* with the default setting.
2. Robust Mahalanobis distance (Rob.Mah; Hyndman and Shang, 2010): the squared robust Mahalanobis distances are calculated by treating the curves as q-dimensional data and the resulting distances follow a χ^2 distribution with q degrees of freedom. A curve is flagged as an outlier if its squared distance is larger than $\chi^2_{0.99,q}$, the critical value. We use *foutliers* in the R package *rainbow* with the default setting.
3. Adjusted Outliergram (Out.Grm; Arribas-Gil and Romo, 2014): the functional boxplot is first applied to detect the magnitude outliers and then the shape outliers are detected by the boxplot of a measurement of shape variation. We use the R code *OutGramAdj* from http://halweb.uc3m.es/esp/Personal/personas/aarribas/esp/public.html.

We consider four models with different types of outliers and different contamination levels $\epsilon = 0$ (uncontaminated), 0.1 and 0.2.

- Model 1 (shifted outlier). Main model: $X(t) = 4t + e(t)$, where $e(t)$ is a Gaussian process with zero mean and covariance function $\gamma(s, t) = \exp\{-|t - s|\}$. Contamination model: $X(t) = 4t + 8U + e(t)$, where U takes values -1 and 1 with probability $1/2$.
- Model 2 (isolated outlier). Main model: $X(t) = 4t + e(t)$ and contamination model: $X(t) = 4t + 8UI_{\{T \leq t \leq T+0.1\}} + e(t)$, where T is generated from a uniform distribution on $[0, 0.9]$ and I_A is an indicator function taking value 1 on set A and 0 otherwise. Models 1 and 2 were considered by Sun and Genton (2011).
- Model 3 (shape outlier I). Main model: $X(t) = 30t(1 - t)^{3/2} + \tilde{e}(t)$, where $\tilde{e}(t)$ is a Gaussian process with zero mean and covariance function $\tilde{\gamma}(s, t) = 0.3 \exp\{-|t - s|/0.3\}$. Contamination model: $X(t) = 30(1 - t)t^{3/2} + \tilde{e}(t)$. This model was considered in Arribas-Gil and Romo (2014).
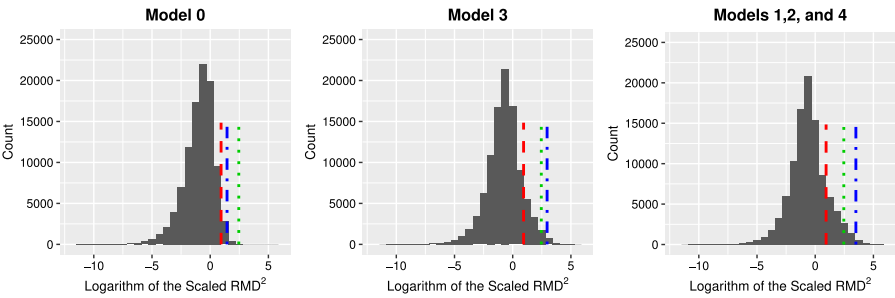
Fig. 4. Histograms of the logarithm of the scaled RMD^2 calculated from the models with different covariance functions. The red dashed line: the 0.993 quantile of the χ^2 distribution with degree of freedom 2. The green dotted line: the 0.993 quantile of the F-distribution with simulated parameters. The blue dash–dot line: the 0.993 empirical quantile of the data. The quantile of the F-distribution is more accurate as the cutoff value.

Table 1

Mean and standard deviation (in parentheses) of the percentage of correctly and falsely detected outliers over 500 simulation runs with four univariate models. **Bold** font is used to highlight the worst performance on both measurements for each setting. Int.Sqe: integrated squared error method; Rob.Mah: robust Mahalanobis distance; Out.Grm: adjusted outliergram; Dir.Out: method based-on directional outlyingness.

Method	Model 1		Model 2		Model 3		Model 4	
	p_c	p_f	p_c	p_f	p_c	p_f	p_c	p_f
$\epsilon = 0$								
Int.Sqe	–	**7.1** (2.7)	–	**7.1** (2.7)	–	**4.1** (2.0)	–	**7.1** (2.7)
Rob.Mah	–	1.5 (1.3)	–	1.5 (1.3)	–	1.5 (1.3)	–	1.5 (1.3)
Out.Grm	–	1.2 (1.2)	–	1.2 (1.2)	–	1.0 (1.3)	–	1.2 (1.2)
Dir.Out	–	1.9 (1.6)	–	1.9 (1.6)	–	1.0 (1.1)	–	1.9 (1.6)
$\epsilon = 0.1$								
Int.Sqe	**37.6** (30.1)	**6.1** (2.6)	100 (0.0)	**6.3** (2.7)	**55.3** (36.8)	3.5 (1.9)	100 (0.0)	**5.8** (2.4)
Rob.Mah	100 (0.0)	0.4 (0.7)	**25.4** (15.5)	0.8 (1.1)	98.9 (4.8)	0.4 (0.8)	**11.8** (10.1)	1.0 (1.3)
Out.Grm	100 (0.0)	2.1 (2.1)	67.8 (20.2)	3.6 (3.2)	82.3 (18.7)	1.9 (1.7)	85.1 (16.3)	3.3 (2.2)
Dir.Out	99.6 (2.1)	1.1 (1.2)	100 (0.0)	1.0 (1.2)	99.8 (1.8)	0.6 (0.9)	98.6 (4.1)	1.0 (1.2)
$\epsilon = 0.2$								
Int.Sqe	**29.9** (24.9)	5.5 (2.8)	100 (0.0)	5.1 (2.6)	43.0 (33.5)	3.1 (1.9)	100 (0.0)	4.8 (2.4)
Rob.Mah	100 (0.0)	0.0 (0.2)	**15.4** (10.2)	0.3 (0.7)	91.5 (12.6)	0.0 (0.1)	**9.2** (6.8)	0.7 (1.0)
Out.Grm	100 (0.2)	**14.7** (9.9)	64.5 (17.4)	**7.9** (5.3)	**29.1** (16.5)	1.2 (1.6)	85.1 (14.9)	**5.1** (2.9)
Dir.Out	99.3 (2.9)	0.4 (0.7)	100 (0.0)	0.3 (0.6)	94.6 (6.8)	0.2 (0.5)	89.5 (12.9)	0.3 (0.7)

- Model 4 (shape outlier II). Main model: $X(t) = 4t + \tilde{e}_1(t)$, where $\tilde{e}_1(t)$ is a Gaussian process with zero mean and covariance function $\gamma_1(s, t) = \exp\{-|t - s|\}$. Contamination model: $X(t) = 4t + \tilde{e}_2(t)$, where $\tilde{e}_2(t)$ is a Gaussian process with zero mean and covariance function $\gamma_2(s, t) = 8 \exp\{-|t - s|^{0.2}\}$. This model was considered by Sun and Genton (2011). The contamination is from the covariance function but eventually leads to different shapes for the two groups.

For each case, we generate 100 curves at 50 equidistant time points on [0, 1]. For the proposed outlier detection procedure, we set $h = [0.75n]$, which means that we assume that the proportion of outliers in a group of curves is no more than 25%. For comparison, we calculate two quantities: the correct detection rate, p_c (number of correctly detected outliers divided by the total number of outlying curves), and the false detection rate, p_f (number of falsely detected outliers divided by the total number of normal curves). The simulation results are presented in Table 1.

For Model 0, the effective spatial range (the lag corresponding to 5% correlation) is about 0.003 and the F-distribution approximates the tail distribution of scaled RMD^2 quite well; see the first plot of Fig. 4. However, Models 1–4 all have long effective spatial ranges of their covariance functions. Specifically, this range is 3 for Models 1, 2, and 4, and 0.9 for Model 3, which are relatively long for the [0, 1] design interval. As a result, the distribution of $(\mathrm{MO}_{T_k, n}, \mathrm{VO}_{T_k, n})^{\mathrm{T}}$ deviates a little from the normal distribution, so the tail distribution of the scaled RMD^2 is not as well approximated as that of Model 0; see the second and third plots of Fig. 4. Nevertheless, our simulation study shows that the cutoff value from the F-distribution still leads to reasonable outlier detection results for such settings. Simulation results for models with short effective spatial ranges are provided in an online supplementary document.

When the model is clean ($\epsilon = 0$), Int.Sqe suffers from high false detection rates compared with the other methods. Each of the three methods performs poorly for either p_c or p_f with the contamination models. In particular, Int.Sqe fails to handle Models 1 and 3, Rob.Mah performs poorly with Models 2 and 4 and Out.Grm produces the highest false detection rate when $\epsilon = 0.2$. It is also not robust to the rising contamination level (see Model 3, p_c for $\epsilon = 0.1$ and 0.2). In contrast, Dir.Out

Table 2

Mean and standard deviation (in parentheses) of the percentage of correctly and falsely recognized outliers over 500 simulation runs with six bivariate models. **Bold** font is used to highlight the worst performance on both measurements for each setting. AdjFB.WMBD: adjusted functional boxplot using weighted modified band depth; AdjFB.MSBD: adjusted functional boxplot using modified simplicial depth; Mar.Dir.Out: detect outliers marginally with Dir.Out and combine them together as the final result; Tot.Dir.Out: detect outliers jointly with Dir.Out.

Method	Model 5		Model 6		Model 7	
	p_c	p_f	p_c	p_f	p_c	p_f
AdjFB.WMBD	–	0.0 (0.0)	**31.7** (15.0)	0.0 (0.0)	83.8 (12.4)	0.0 (0.0)
AdjFB.MSBD	–	0.0 (0.0)	63.0 (15.6)	0.0 (0.0)	**74.1** (16.3)	0.0 (0.0)
Mar.Dir.Out	–	**2.0** (0.5)	100 (0.0)	0.0 (0.0)	100 (0.0)	**0.0** (0.2)
Tot.Dir.Out	–	0.0 (0.2)	100 (0.0)	**0.0** (0.2)	100 (0.0)	**0.0** (0.2)

Method	Model 8		Model 9		Model 10	
	p_c	p_f	p_c	p_f	p_c	p_f
AdjFB.WMBD	**0.0** (0.0)	0.0 (0.0)	**0.0** (0.0)	0.0 (0.0)	**0.0** (0.0)	0.0 (0.0)
AdjFB.MSBD	**0.0** (0.0)	0.0 (0.0)	**0.0** (0.0)	0.0 (0.0)	**0.0** (0.0)	0.0 (0.0)
Mar.Dir.Out	59.6 (17.7)	0.0 (0.0)	81.6 (12.7)	0.0 (0.0)	66.1 (16.6)	0.0 (0.1)
Tot.Dir.Out	83.2 (13.0)	**0.0** (0.1)	93.7 (7.6)	**0.0** (0.1)	81.8 (13.4)	**0.0** (0.1)

generates quite stable and satisfying correct detection rates with a low false detection rate. All these results indicate that our proposed method based on directional outlyingness can detect various types of outliers.

5.2. Multivariate functional data

For multivariate functional data, we consider WMBD (Ieva and Paganoni, 2013) and MSBD (López-Pintado et al., 2014) as two competitors. WMBD is constructed as a weighted average of the marginal modified band depth of each variable of the multivariate functional data. The adjusted functional boxplot (Sun and Genton, 2012) based on WMBD is applied to detect marginal outliers and the final result is the union of these marginal outliers. MSBD is defined as the mean of point-wise simplicial depths across the whole design interval. We follow the outlier detection procedure based on MSBD from López-Pintado et al. (2014). For our method, we apply it in two ways: (1) treating each variable as a univariate curve, detecting marginal outliers and combining them together as the final result (Mar.Dir.Out); (2) taking bivariate curves as a whole and detecting the overall outliers (Tot.Dir.Out).

We consider six groups of bivariate curves containing outliers with different types and levels of outlyingness. Following the setting in López-Pintado et al. (2014), we define the main model as $\mathbf{X}(t) = \mathbf{e}(t)$, where $\mathbf{e}(t) = \{e_1(t), e_2(t)\}^T$ is a bivariate Gaussian process with zero mean and cross-covariance function (Gneiting et al., 2010; Apanasovich et al., 2012):

$$C_{ij}(s, t) = \rho_{ij}\sigma_i\sigma_j\mathcal{M}(|s - t|; \nu_{ij}, \alpha_{ij}), \quad i, j = 1, 2,$$

where ρ_{12} is the correlation between $X_1(t)$ and $X_2(t)$, $\rho_{11} = \rho_{22} = 1$, σ_i^2 is the marginal variance and $\mathcal{M}(h; \nu, \alpha) = 2^{1-\nu}\Gamma(\nu)^{-1}(\alpha|h|)^\nu \mathcal{K}_\nu(\alpha|h|)$ with $|h| = |s - t|$, is the Matérn class (Matérn, 1960) where $\mathcal{K}_\nu$ is a modified Bessel function of the second kind, $\nu > 0$ is a smoothness parameter, and $\alpha > 0$ is a range parameter. Throughout the simulation, we choose the following parameters for the bivariate Matérn cross-covariance function: $\sigma_1 = \sigma_2 = 1$, $\alpha_{11} = 0.02$, $\alpha_{22} = 0.01$, $\alpha_{12} = 0.016$, $\nu_{11} = 1.2$, $\nu_{22} = 0.6$, $\nu_{12} = 1$ and $\rho_{12} = 0.6$. The six models investigated are as follows:

- Model 5 (uncontaminated model). Main model: $\mathbf{X}(t) = \mathbf{e}(t)$.
- Model 6 (consistent outlier). Main model: $\mathbf{X}(t) = \mathbf{e}(t)$ and contamination model: $X_i(t) = 4e_i(t)$, $i = 1, 2$.
- Model 7 (isolated outlier). Main model: $\mathbf{X}(t) = \mathbf{e}(t)$ and contamination model: $X_i(t) = e_i(t)(1+11I_{\{T \leq t \leq T+0.1\}})$, $i = 1, 2$.
- Model 8 (weak consistent outlier). Main model: $\mathbf{X}(t) = \mathbf{e}(t)$ and contamination model: $X_1(t) = 1.7e_1(t)$ and $X_2(t) = 1.5e_2(t)$. This is a weak version of Model 6.
- Model 9 (weak isolated outlier). Main model: $\mathbf{X}(t) = \mathbf{e}(t)$ and contamination model: $X_i(t) = e_i(t)(1 + 4I_{\{T \leq t \leq T+0.1\}})$, $i = 1, 2$. This is a weak version of Model 7.
- Model 10 (shape outlier). Main model: $X_1(t) = e_1(t) + U_{11}\cos(4\pi t)$ and $X_2(t) = e_2(t) + U_{12}\sin(4\pi t)$, where U_{11} and U_{12} are independent and follow a uniform distribution on [2, 3]; contamination model: $X_1(t) = e_1(t) + U_{21}\cos(4\pi t)$ and $X_2(t) = e_2(t) + U_{22}\sin(4\pi t)$, where U_{21} and U_{22} are independent and follow a uniform distribution on [3.2, 3.5].

We set the contamination level in the contamination models to $\epsilon = 0.1$. For each case, we generate 100 bivariate curves on 50 equally spaced time points on [0, 1]. The same $h = [0.75n]$ is employed. The correct detection rate, p_c, and false detection rate, p_f, are calculated and reported in Table 2. For all six models, the four methods are quite satisfactory by generating small p_f. For Models 6 and 7, the proposed two methods perfectly detect all the outliers, a result much better than the results from the two competitors. For Models 8, 9 and 10, WMBD and MSBD fail to detect any outlier due to the conservativeness of the functional boxplot. Furthermore, for these three models, Tot.Dir.Out has significant improvement over Mar.Dir.Out, which suggests that it is indeed better to treat the bivariate curves as a whole when detecting outliers.
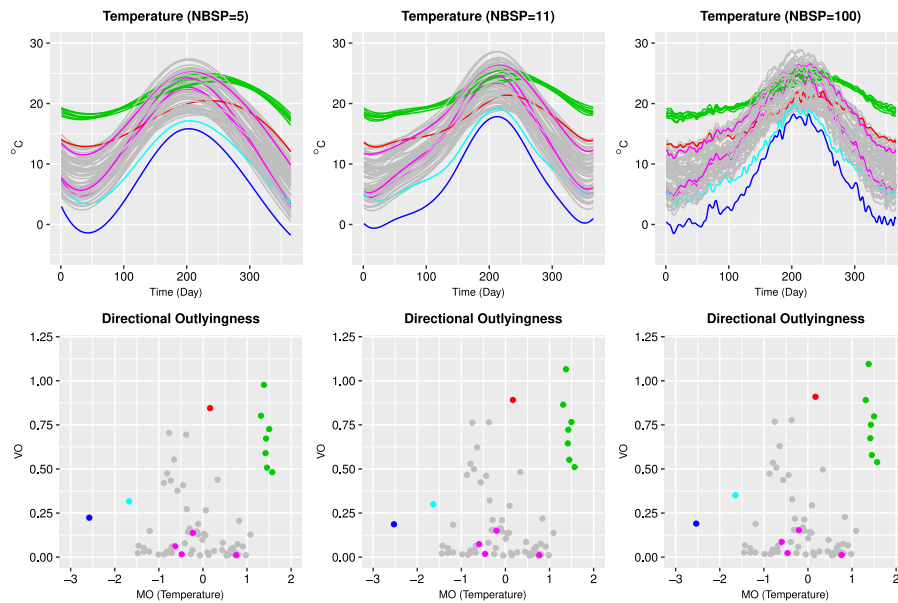
Fig. 5. Top panel: temperature curves smoothed with different numbers of B-spline basis functions (NBSP). Bottom panel: directional outlyingness plot corresponding to the fitted curves.

6. Data applications

6.1. Spanish weather data

Besides simulations, we test our proposed framework with two datasets. The first dataset is Spanish weather data from the R package *fda.usc*. This dataset contains geographic information of 73 weather stations in Spain, from where average daily temperature and daily log precipitation for the period 1980–2009 were recorded. The data are discretely observed and hence smoothed with 11 order-4 B-spline basis functions. According to our experience, the plot of $(\mathbf{MO}^{\mathrm{T}}, \mathrm{VO})^{\mathrm{T}}$ is quite robust to the amount of smoothing (see Fig. 5) and to the choice of smoothing methods (see Figure S1 of the supplementary material.)

We separate the stations into six groups mainly with respect to their geographic locations, which have great influence on the weather and check if the proposed method can also distinguish such groups based on the weather records. Specifically, we calculate the functional directional outlyingness for the temperature curves, the log precipitation curves, and the bivariate curves combining two types of data together, respectively. We then illustrate the results for the three cases (Fig. 6). For the univariate cases, we see clear patterns from the directional outlyingness plot corresponding with the magnitudes and shapes of the curves. For instance, the seven green and two blue temperature curves are mapped as points isolated from the main cluster (Fig. 6, top) and the green and purple log precipitation curves are also well distinguished in the directional outlyingness plot (Fig. 6, middle). For the bivariate case, all the six groups of stations are clearly located in the directional outlyingness plot. These results demonstrate that the functional directional outlyingness provides an effective way to visualize the centrality of functional data.

6.2. ECG data

The second dataset consists of electrocardiogram (ECG) data, which is a measure of how the electrical activity of the heart changes over time as action potentials propagate throughout the heart during each cardiac cycle. ECG data are used to conduct heartbeat classification to diagnose abnormalities in heart activities. We obtained the data from the MIT-BIH Arrhythmia Database (Goldberger et al., 2000) and Wei and Keogh (2006). The data were annotated by cardiologists and a label of *normal* or *abnormal* was assigned to each data record; see Fig. 7.

All the data records were normalized and rescaled to have lengths of 85. We took all the training samples in Wei and Keogh (2006) including 208 abnormal and 602 normal cases. Only observations on time points 6 to 80 were considered to avoid boundary effects. We detected abnormal curves (outliers) with six methods including the four methods used in Sections 5.1 and 6.1, the functional directional outlyingness method based on both the mean function and the first-order derivative function (Dir.Out1), and the functional directional outlyingness method based on the mean function, the first- and second-order derivative functions (Dir.Out2). We randomly selected 400 curves from the total 810 observations, controlling the contamination level (CL) at 0, 5%, 10%, 15%, 20% and 25%, respectively. The CL of the raw data is 25.7%, so we set the
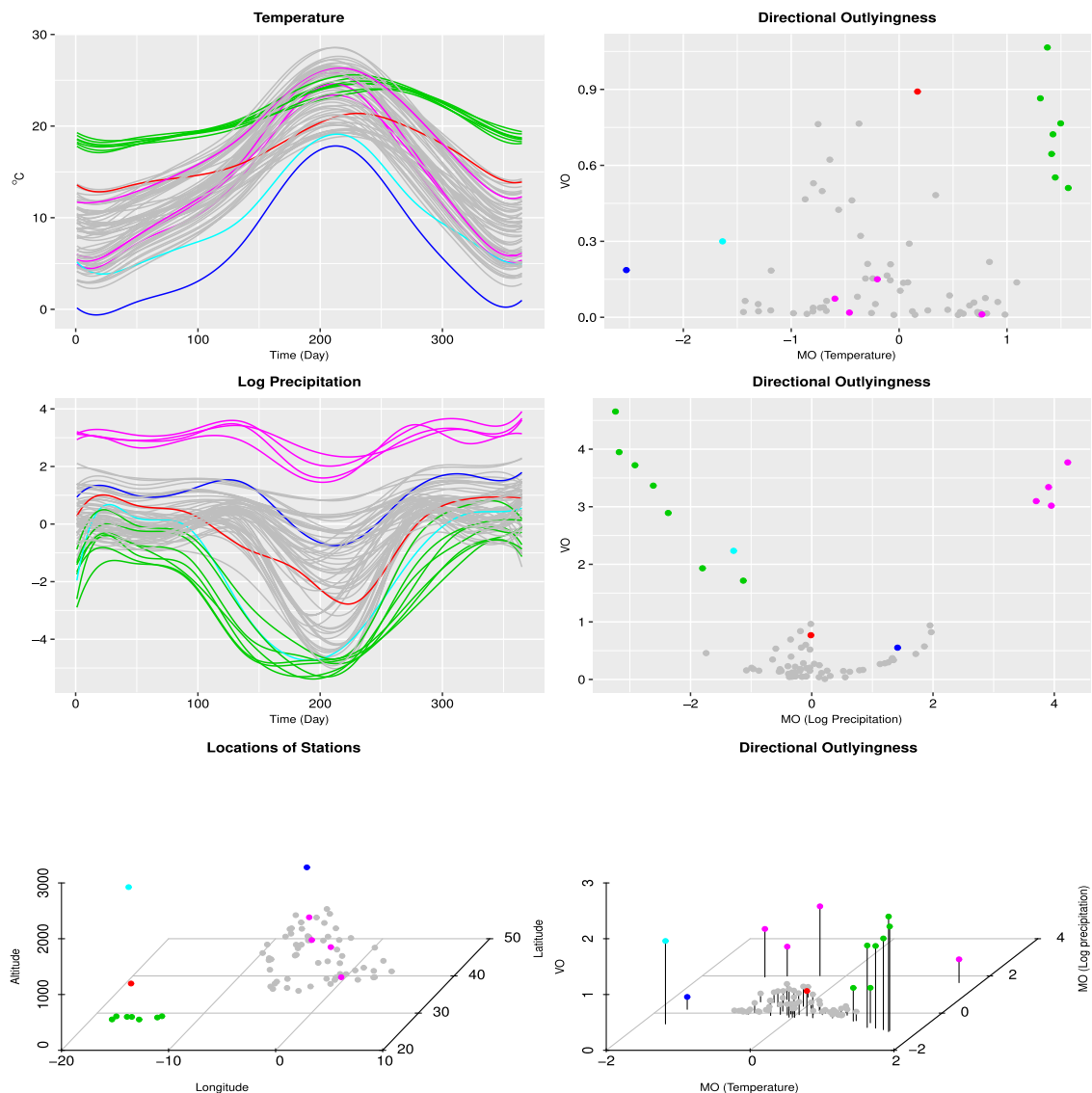
Fig. 6. Top panel: temperature curves (left) and directional outlyingness plot (right); middle panel: log precipitation curves (left) and directional outlyingness plot (right); bottom panel: locations of stations (left) and directional outlyingness plot for bivariate curves (right). Colors represent different groups of outlying curves. (For interpretation of the references to color in this figure legend, the reader is referred to the web version of this article.)

maximum CL as 25%. The 400 curves were selected in this way: when CL is 10%, for example, we randomly chose 40 from 208 abnormal curves and 360 from 602 normal curves. For each CL, we calculated the detection rates, p_c and p_f, for each method. We repeated this procedure for 50 times and report the average rates in Table 3.

First of all, Out.Grm and Rob.Mah are not acceptable due to their poor correct detection rate when CL > 0. When CL = 0, Int.Sqe and Dir.Out all suffer from high false detection rates because even the normal curves (gray ones in Fig. 7) demonstrate significantly different patterns (the segment between times 20 and 40 for example). That is to say, although these people are diagnosed as normal, some individual differences of heart activities still exist among them. As CL increases, Dir.Out type methods reduce the false detection rate more rapidly than Int.Sqe. For the correct detection rate, Int.Sqe is better than Dir.Out but worse than Dir.Out1 and Dir.Out2. These results indicate that it is better to consider the derivative functions together with the mean function in practical implementations of the outlier detection method based on directional outlyingness.

We also compared the computational speeds of the six methods by applying them to the whole 810 curves. The results are reported in Table 4. Int.Sqe is shown to take the longest time, which is about 240 times slower than the fastest method, Dir.Out. After increasing the dimension of curves, Dir.Out1 and Dir.Out2 take longer time than Dir.Out since the calculation of depth for multivariate data is more time-consuming than for univariate data. Nevertheless, Dir.Out1 and Dir.Out2 are still much faster than Int.Sqe.
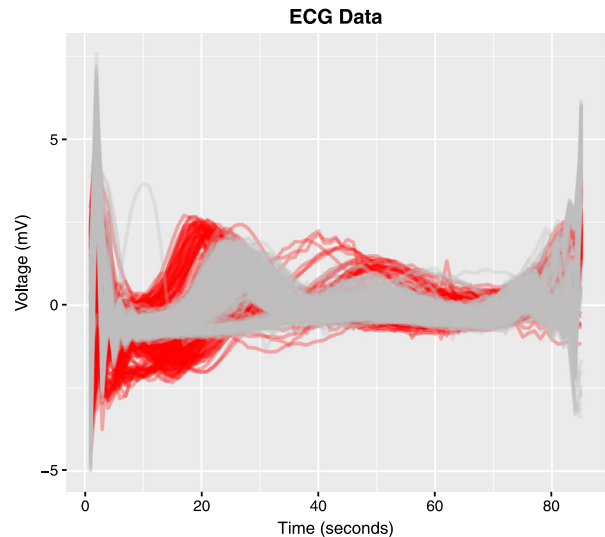
Fig. 7. The ECG data: normal curves (gray); abnormal curves (red). (For interpretation of the references to color in this figure legend, the reader is referred to the web version of this article.)

Table 3
A comparison of the outlier detection performances of the six methods applied to the ECG data of different contamination levels (CL). Int.Sqe: integrated squared error method; Rob.Mah: robust Mahalanobis distance; Out.Grm: adjusted outliergram; Dir.Out, Dir.Out1, and Dir.Out2: methods based-on directional outlyingness.

CL	Rate	Int.Sqe	Rob.Mah	Out.Grm	Dir.Out	Dir.Out1	Dir.Out2
0	p_c	–	–	–	–	–	–
	p_f	16.7	13.1	5.3	17.3	18.0	20.3
5%	p_c	96.0	48.7	67.3	90.1	99.3	100
	p_f	16.6	13.0	4.9	15.6	15.2	17.3
10%	p_c	93.3	39.7	56.3	86.9	98.2	99.5
	p_f	15.7	12.4	4.0	12.8	12.4	12.3
15%	p_c	90.9	28.6	46.0	81.7	96.4	99.2
	p_f	15.3	11.2	3.2	10.0	11.0	10.4
20%	p_c	85.3	20.0	33.8	74.1	93.1	97.5
	p_f	14.2	8.3	2.3	7.3	8.4	7.2
25%	p_c	76.6	7.1	19.6	60.4	86.1	92.9
	p_f	12.9	1.6	1.7	4.2	5.8	5.8

Table 4
A comparison of the computational speeds of the six methods applied to the ECG data.

	Int.Sqe	Out.Grm	Rob.Mah	Dir.Out	Dir.Out1	Dir.Out2
Time (s)	144.7	20.7	3.5	0.6	15.4	17.7

7. Discussion

Unlike with point-wise data, the direction of outlyingness is crucial to describing the centrality of multivariate functional data. Motivated by this, we proposed a new framework of directional outlyingness for multivariate functional data by taking the direction of outlyingness into consideration. Compared with classical functional depth, functional directional outlyingness reveals its superiority by naturally decomposing the total outlyingness into two parts: magnitude outlyingness and shape outlyingness, and by visualizing the centrality of a group of curves. We created an outlier detection criterion, applicable to both univariate and multivariate curves, based on functional directional outlyingness. This criterion outperformed competing methods in simulation studies. Moreover, all methods proposed here can be readily extended to the case where the design area is two-dimensional, corresponding to image data (Genton et al., 2014).

Most classical functional depths map a curve (both univariate and multivariate) to a univariate depth curve (a sequence of nonnegative scalar depth, discretely). Most existing methods can be derived from various ways of dealing with such a depth curve. For example, by taking the weighted average across the design interval, we obtain ID, MBD, MSBD, MHD and MFHD; by taking the smallest value of the depth curve, we obtain BD, HD and SBD; by stochastically ordering the left tail of

the distributions of these point-wise depths, we obtain the extremal depth. However, the functional directional outlyingness maps each curve to an outlyingness curve (or a sequence of vectors, discretely) of the same dimension. This preservation of dimension provides much more information and flexibility for functional data visualization and outlier detection. In the current paper, we made use of this sequence of vectors in two different ways: taking their weighted average leads to **MO** and calculating their variance leads to VO. Other ways of handling this sequence are to be further explored, so that different measures for the centrality of functional data can be obtained for various purposes.

Another good feature of functional directional outlyingness is the outlyingness decomposition, which allows us to demonstrate the centrality of the curves and also the type of outliers more accurately. Similar ideas have been proposed based on classical point-wise depth in the literature. Hubert et al. (2015) proposed multivariate functional skew-adjusted projection depth (MFSPD) to be a weighted average of point-wise, skew-adjusted projection depth (SPD). They used $1 - \text{MFSPD}$ as the overall depth and treated the difference between the harmonic mean and the arithmetic mean of the point-wise SPD as the shape depth. Hubert et al. (2016) measured overall outlyingness with the weighted average of point-wise adjusted outlyingness (AO) and the shape outlyingness with the scaled standard deviation of AO. However, their decomposition is less natural in that the two components are dependent on each other, and also their measurements of the shape depth (outlyingness) is less accurate compared with our VO due to the lack of the direction of outlyingness, a fact also discussed by Narisetty and He (2015).

Acknowledgments

Appendix A

Proof of Theorem 1. We provide a proof of the first property. Proofs of the other two properties can be directly derived using definition (3) and the properties of $d\left(\mathbf{X}(t), F_{\mathbf{X}(t)}\right)$. We have $d\left(\mathbf{A}\mathbf{X}(t) + \mathbf{b}, F_{\mathbf{A}\mathbf{X}(t)+\mathbf{b}}\right) = d\left(\mathbf{X}(t), F_{\mathbf{X}(t)}\right)$ and $d\left(\mathbf{A}\mathbf{Z}(t) + \mathbf{b}, F_{\mathbf{A}\mathbf{X}(t)+\mathbf{b}}\right) = d\left(\mathbf{Z}(t), F_{\mathbf{X}(t)}\right)$ based-on the affine invariance of $d\left(\mathbf{X}(t), F_{\mathbf{X}(t)}\right)$. Hence, $\|\mathbf{O}\left(\mathbf{A}\mathbf{X}(t) + \mathbf{b}, F_{\mathbf{A}\mathbf{X}(t)+\mathbf{b}}\right)\| = \|\mathbf{O}\left(\mathbf{X}(t), F_{\mathbf{X}(t)}\right)\|$. For the direction of this outlyingness, we have

$$\mathbf{v}^*(t) = \frac{\mathbf{A}\mathbf{X}(t) - \mathbf{A}\mathbf{Z}(t)}{\|\mathbf{A}\mathbf{X}(t) - \mathbf{A}\mathbf{Z}(t)\|} = \frac{\mathbf{A}\|\mathbf{X}(t) - \mathbf{Z}(t)\|}{\|\mathbf{A}\mathbf{X}(t) - \mathbf{A}\mathbf{Z}(t)\|} \cdot \frac{\mathbf{X}(t) - \mathbf{Z}(t)}{\|\mathbf{X}(t) - \mathbf{Z}(t)\|} = \mathbf{U} \cdot \mathbf{v}(t).$$

By the definition of $\mathbf{v}^*(t)$, we have

$$\begin{aligned}
\mathbf{O}\left(\mathbf{A}\mathbf{X}(t) + \mathbf{b}, F_{\mathbf{A}\mathbf{X}(t)+\mathbf{b}}\right) &= \mathbf{v}^*(t)\|\mathbf{O}\left(\mathbf{A}\mathbf{X}(t) + \mathbf{b}, F_{\mathbf{A}\mathbf{X}(t)+\mathbf{b}}\right)\| \\
&= \mathbf{U} \cdot \mathbf{v}(t)\|\mathbf{O}\left(\mathbf{X}(t), F_{\mathbf{X}(t)}\right)\| = \mathbf{U} \cdot \mathbf{O}\left(\mathbf{X}(t), F_{\mathbf{X}(t)}\right).
\end{aligned}$$

This completes the proof. □

Proof of Theorem 2. With the consistency of the median, we get $\mathbf{v}_n(t) \to \mathbf{v}(t)$. Then, combined with the convergence of classical depth, we get the consistency of directional outlyingness. □

Proof of Theorem 3. We decompose the total outlyingness into two parts: magnitude outlyingness and shape outlyingness:

$$\begin{aligned}
\text{FO}(\mathbf{X}, F_{\mathbf{X}}) &= \int_{\mathcal{I}} \|\mathbf{O}(\mathbf{X}(t), F_{\mathbf{X}(t)})\|^2 w(t)\mathrm{d}t \\
&= \int_{\mathcal{I}} \|\mathbf{O}(\mathbf{X}(t), F_{\mathbf{X}(t)}) - \mathbf{MO}(\mathbf{X}, F_{\mathbf{X}}) + \mathbf{MO}(\mathbf{X}, F_{\mathbf{X}})\|^2 w(t)\mathrm{d}t \\
&= \int_{\mathcal{I}} \|\mathbf{O}(\mathbf{X}(t), F_{\mathbf{X}(t)}) - \mathbf{MO}(\mathbf{X}, F_{\mathbf{X}})\|^2 w(t)\mathrm{d}t + \|\mathbf{MO}(\mathbf{X}, F_{\mathbf{X}})\|^2 \\
&= \text{VO}(\mathbf{X}, F_{\mathbf{X}}) + \|\mathbf{MO}(\mathbf{X}, F_{\mathbf{X}})\|^2. \quad \square
\end{aligned}$$

Proof of Theorem 4. 1(a) Since g is a one-to-one transformation on the interval $\mathcal{I}$,

$$\begin{aligned}
\text{FO}\left(\mathbf{X}_g, F_{\mathbf{X}_g}\right) &= \int_{\mathcal{I}} \|\mathbf{O}\left(\mathbf{X}\{g(t)\}, F_{\mathbf{X}\{g(t)\}}\right)\|^2 w\{g(t)\}\mathrm{d}t \\
&= \int_{g^{-1}(\mathcal{I})} \|\mathbf{O}\left(\mathbf{X}(t), F_{\mathbf{X}(t)}\right)\|^2 w(t)\mathrm{d}t = \text{FO}\left(\mathbf{X}, F_{\mathbf{X}}\right).
\end{aligned}$$

Also, we have $\text{FO}\left(\mathbf{X}_g, F_{\mathbf{X}_g}\right) = \text{FO}\left(\mathbf{T}(\mathbf{X}_g), F_{\mathbf{T}(\mathbf{X}_g)}\right)$ by the affine invariance of $\mathbf{O}(\mathbf{X}(t), F_{\mathbf{X}(t)})$. Consequently, we proved that $\text{FO}\left(\mathbf{T}(\mathbf{X}_g), F_{\mathbf{T}(\mathbf{X}_g)}\right) = \text{FO}\left(\mathbf{X}, F_{\mathbf{X}}\right)$.

1(b) By a similar procedure with 1(a), we can show

$$\mathbf{MO}\left(\mathbf{T}(\mathbf{X}), F_{\mathbf{T}(\mathbf{X})}\right) = \mathbf{MO}\left(\mathbf{T}(\mathbf{X}_g), F_{\mathbf{T}(\mathbf{X}_g)}\right). \tag{5}$$

By the proof of Theorem 1, we get

$$\mathbf{O}(\mathbf{T}(\mathbf{X}(t)), F_{\mathbf{T}(\mathbf{X}(t))}) = \frac{f(t)\mathbf{A}_0\|\mathbf{X}(t) - \mathbf{Z}(t)\|}{\|f(t)\| \cdot \|\mathbf{A}_0\{\mathbf{X}(t) - \mathbf{Z}(t)\}\|} \mathbf{O}(\mathbf{X}(t), F_{\mathbf{X}(t)}),$$

and $\|\mathbf{X}(t) - \mathbf{Z}(t)\| = \|\mathbf{A}_0\{\mathbf{X}(t) - \mathbf{Z}(t)\}\|$ by noting that $\mathbf{A}_0$ is an orthogonal matrix. Thus

$$\begin{aligned}
\mathbf{MO}(\mathbf{T}(\mathbf{X}), F_{\mathbf{T}(\mathbf{X})}) &= [\lambda(\mathcal{I})]^{-1} \int_{\mathcal{I}} \mathbf{O}(\mathbf{T}(\mathbf{X}(t)), F_{\mathbf{T}(\mathbf{X}(t))}) \mathrm{d}t \\
&= [\lambda(\mathcal{I})]^{-1} \int_{\mathcal{I}} \frac{f(t)}{\|f(t)\|} \mathbf{A}_0 \cdot \mathbf{O}(\mathbf{X}(t), F_{\mathbf{X}(t)}) \mathrm{d}t \\
&= \mathbf{A}_0 \cdot \mathbf{MO}(\mathbf{X}(t), F_{\mathbf{X}(t)}).
\end{aligned} \tag{6}$$

With (5) and (6), we get $\mathbf{MO}\left(\mathbf{T}(\mathbf{X}_g), F_{\mathbf{T}(\mathbf{X}_g)}\right) = \mathbf{A}_0 \cdot \mathbf{MO}(\mathbf{X}(t), F_{\mathbf{X}(t)})$.

Consequently, we have $\mathrm{VO}(\mathbf{T}(\mathbf{X}_g), F_{\mathbf{T}(\mathbf{X}_g)}) = \mathrm{VO}(\mathbf{X}(t), F_{\mathbf{X}(t)})$. Properties 2 and 3 are immediate results from the properties of $\|\mathbf{O}\|$ in Theorem 1. $\square$

Proof of Theorem 5.

$$\sup_{\mathbf{X} \in (\mathbb{R}^p)^k} \|\mathbf{MO}_{T_k, n}\left(\mathbf{X}, F_{\mathbf{X}, n}\right) - \mathbf{MO}_{T_k}\left(\mathbf{X}, F_{\mathbf{X}}\right)\| = \sup_{\mathbf{X} \in (\mathbb{R}^p)^k} \left\| \frac{1}{k} \sum_{i=1}^{k} \left\{ \mathbf{O}_n\left(\mathbf{X}(t_i), F_{\mathbf{X}(t_i), n}\right) w_n(t_i) - \mathbf{O}\left(\mathbf{X}(t_i), F_{\mathbf{X}(t_i)}\right) w(t_i) \right\} \right\|$$

$$\leq \sup_{\mathbf{X} \in (\mathbb{R}^p)^k} \left\| \frac{1}{k} \sum_{i=1}^{k} \left\{ \mathbf{O}_n\left(\mathbf{X}(t_i), F_{\mathbf{X}(t_i), n}\right) - \mathbf{O}\left(\mathbf{X}(t_i), F_{\mathbf{X}(t_i)}\right) \right\} w_n(t_i) \right\| + \sup_{\mathbf{X} \in (\mathbb{R}^p)^k} \left\| \frac{1}{k} \sum_{i=1}^{k} \mathbf{O}\left(\mathbf{X}(t_i), F_{\mathbf{X}(t_i)}\right) \{w_n(t_i) - w(t_i)\} \right\|.$$

By convergence of $\mathbf{O}_n$ and $w_n(t_i), t_i \in T_k$, we get the uniform, almost sure convergence of $\mathbf{MO}_{T_k, n}$ to $\mathbf{MO}_{T_k}$. $\square$

Appendix B. Supplementary data

Supplementary material related to this article can be found online at https://doi.org/10.1016/j.csda.2018.03.017.

References

Apanasovich, T.V., Genton, M.G., Sun, Y., 2012. A valid Matérn class of cross-covariance functions for multivariate random fields with any number of components. J. Amer. Statist. Assoc. 107, 180–193.

Arribas-Gil, A., Romo, J., 2014. Shape outlier detection and visualization for functional data: the outliergram. Biostatistics 15, 603–619.

Chakraborty, A., Chaudhuri, P., 2014a. On data depth in infinite dimensional spaces. Ann. Inst. Statist. Math. 66, 303–324.

Chakraborty, A., Chaudhuri, P., 2014b. The spatial distribution in infinite dimensional spaces and related quantiles and depths. Ann. Statist. 42, 1203–1231.

Claeskens, G., Hubert, M., Slaets, L., Vakili, K., 2014. Multivariate functional halfspace depth. J. Amer. Statist. Assoc. 109, 411–423.

Cuevas, A., Febrero, M., Fraiman, R., 2006. On the use of the bootstrap for estimating functions with functional data. Comput. Statist. Data Anal. 51, 1063–1074.

Cuevas, A., Fraiman, R., 2009. On depth measures and dual statistics. A methodology for dealing with general data. J. Multivariate Anal. 100, 753–766.

Donoho, D.L., 1982. Breakdown Properties of Multivariate Location Estimators. (Ph. D. Qualifying paper), Harvard University.

Febrero, M., Galeano, P., González-Manteiga, W., 2008. Outlier detection in functional data by depth measures, with application to identify abnormal NOx levels. Environmetrics 19, 331–345.

Ferraty, F., Vieu, P., 2006. Nonparametric Functional Data Analysis: Theory and Practice. Springer.

Fraiman, R., Muniz, G., 2001. Trimmed means for functional data. TEST 10, 419–440.

Genton, M.G., Johnson, C., Potter, K., Stenchikov, G., Sun, Y., 2014. Surface boxplots. Stat 3, 1–11.

Gervini, D., 2009. Detecting and handling outlying trajectories in irregularly sampled functional datasets. Ann. Appl. Stat. 3, 1758–1775.

Gervini, D., 2012. Outlier detection and trimmed estimation for general functional data. Statist. Sinica 22, 1639–1660.

Gijbels, I., Nagy, S., 2015. Consistency of non-integrated depths for functional data. J. Multivariate Anal. 140, 259–282.

Gneiting, T., Kleiber, W., Schlather, M., 2010. Matérn cross-covariance functions for multivariate random fields. J. Amer. Statist. Assoc. 105, 1167–1177.

Goldberger, A.L., Amaral, L.A., Glass, L., Hausdorff, J.M., Ivanov, P.C., Mark, R.G., Mietus, J.E., Moody, G.B., Peng, C.-K., Stanley, H.E., 2000. Physiobank, physiotoolkit, and physionet components of a new research resource for complex physiologic signals. Circulation 101, e215–e220.

Hardin, J., Rocke, D.M., 2005. The distribution of robust distances. J. Comput. Graph. Statist. 14, 928–946.

Hong, Y., Davis, B., Marron, J., Kwitt, R., Singh, N., Kimbell, J.S., Pitkin, E., Superfine, R., Davis, S.D., Zdanski, C.J., et al., 2014. Statistical atlas construction via weighted functional boxplots. Med. Image Anal. 18, 684–698.

Horváth, L., Kokoszka, P., 2012. Inference for Functional Data with Applications. Springer.

Huang, H., Sun, Y., 2016. Total variation depth for functional data. arXiv preprint arXiv:1611.04913.

Hubert, M., Raymaekers, J., Rousseeuw, P.J., Segaert, P., 2016. Finding outliers in surface data and video. arXiv preprint arXiv:1601.08133.

Hubert, M., Rousseeuw, P.J., Segaert, P., 2015. Multivariate functional outlier detection. Stat. Methods Appl. 24, 177–202.

Hyndman, R.J., Shang, H.L., 2010. Rainbow plots, bagplots, and boxplots for functional data. J. Comput. Graph. Statist. 19, 29–45.

Hyndman, R.J., Ullah, M.S., 2007. Robust forecasting of mortality and fertility rates: a functional data approach. Comput. Statist. Data Anal. 51, 4942–4956.

Ieva, F., Paganoni, A.M., 2013. Depth measures for multivariate functional data. Comm. Statist. Theory Methods 42, 1265–1276.

Liu, R.Y., 1990. On a notion of data depth based on random simplices. Ann. Statist. 18, 405–414.

Long, J.P., Huang, J.Z., 2015. A study of functional depths. arXiv preprint arXiv:1506.01332v3.

López-Pintado, S., Romo, J., 2006. Depth-based classification for functional data. In: DIMACS Series in Discrete Mathematics and Theoretical Computer Science. Data Depth: Robust Multivariate Analysis, Computational Geometry and Applications, Vol. 72. pp. 103–120.

López-Pintado, S., Romo, J., 2009. On the concept of depth for functional data. J. Amer. Statist. Assoc. 104, 718–734.

López-Pintado, S., Romo, J., 2011. A half-region depth for functional data. Comput. Statist. Data Anal. 55, 1679–1695.

López-Pintado, S., Sun, Y., Lin, J.K., Genton, M.G., 2014. Simplicial band depth for multivariate functional data. Adv. Data Anal. Classif. 8, 321–338.

Mahalanobis, P.C., 1936. On the generalized distance in statistics. Proc. Natl. Inst. Sci. India 2, 49–55.

Matérn, B., 1960. Spatial Variation. Springer.

McKeague, I.W., López-Pintado, S., Hallin, M., Šiman, M., 2011. Analyzing growth trajectories. J. Dev. Orig. Health Dis. 2, 322–329.

Möttönen, J., Oja, H., 1995. Multivariate spatial sign and rank methods. J. Nonparametr. Stat. 5, 201–213.

Myllymäki, M., Mrkvička, T., Grabarnik, P., Seijo, H., Hahn, U., 2017. Global envelope tests for spatial processes. J. R. Stat. Soc. Ser. B Stat. Methodol. 79, 381–404.

Nagy, S., Gijbels, I., Hlubinka, D., 2016a. Weak convergence of discretely observed functional data with applications. J. Multivariate Anal. 146, 46–62.

Nagy, S., Gijbels, I., Omelka, M., Hlubinka, D., 2016b. Integrated depth for functional data: statistical properties and consistency. ESAIM Probab. Stat. 20, 95–130.

Narisetty, N.N., He, X., 2015. Discussion of "multivariate functional outlier detection". Stat. Methods Appl. 24, 209–215.

Narisetty, N.N., Nair, V.N., 2016. Extremal depth for functional data and applications. J. Amer. Statist. Assoc. 111, 1705–1714.

Ngo, D., Sun, Y., Genton, M.G., Wu, J., Srinivasan, R., Cramer, S.C., Ombao, H., 2015. An exploratory data analysis of electroencephalograms using the functional boxplots approach. Front. Neuroinf. 9, 282.

Nieto-Reyes, A., Battey, H., 2016. A topologically valid definition of depth for functional data. Stat. Sci. 31, 61–79.

Ramsay, J.O., Silverman, B.W., 2005. Functional Data Analysis. Springer.

Rousseeuw, P.J., 1985. Multivariate estimation with high breakdown point. In: Grossmann, W., Pflug, G., Vincze, I., Wert, W. (Eds.), In Mathematical Statistics and Applications, Volume B. Reidel, Dordrecht, pp. 283–297.

Serfling, R., 2006. Depth functions in nonparametric multivariate inference. In: Liu, R.Y., Serfling, R., Souvaine, D.L. (Eds.), In Data Depth: Robust Multivariate Analysis, Computational Geometry and Applications, Vol. 72. American Mathematical Society, pp. 1–16.

Serfling, R., 2010. Equivariance and invariance properties of multivariate quantile and related functions, and the role of standardisation. J. Nonparametr. Stat. 22, 915–936.

Serfling, R., Wijesuriya, U., 2017. Depth-based nonparametric description of functional data, with emphasis on use of spatial depth. Comput. Statist. Data Anal. 105, 24–45.

Stahel, W.A., 1981. Breakdown of covariance estimators. Research Report 31, Fachgruppe für Statistik, ETH, Zürich.

Sun, Y., Genton, M.G., 2011. Functional boxplots. J. Comput. Graph. Statist. 20, 316–334.

Sun, Y., Genton, M.G., 2012. Adjusted functional boxplots for spatio-temporal data visualization and outlier detection. Environmetrics 23, 54–64.

Tukey, J.W., 1975. Mathematics and the picturing of data. In: Proceedings of the International Congress of Mathematicians, Vol. 2, pp. 523–531.

Vardi, Y., Zhang, C.-H., 2000. The multivariate L_1-median and associated data depth. Proc. Natl. Acad. Sci. 97, 1423–1426.

Wei, L., Keogh, E., 2006. Semi-supervised time series classification. In: Proceedings of the 12th ACM SIGKDD International Conference on Knowledge Discovery and Data Mining. ACM, pp. 748–753.

Yu, G., Zou, C., Wang, Z., 2012. Outlier detection in functional observations with applications to profile monitoring. Technometrics 54, 308–318.

Zuo, Y., 2003. Projection-based depth functions and associated medians. Ann. Statist. 31, 1460–1490.

Zuo, Y., Serfling, R., 2000. General notions of statistical depth function. Ann. Statist. 28, 461–482.